Science
AAAS

Measuring the Cosmic-Ray Acceleration Efficiency of a Supernova Remnant
E. A. Helder, *et al.*
Science **325**, 719 (2009);
DOI: 10.1126/science.1173383

Science (print ISSN 0036-8075; online ISSN 1095-9203) is published weekly, except the last week in December, by the American Association for the Advancement of Science, 1200 New York Avenue NW, Washington, DC 20005.

Measuring the Cosmic-Ray Acceleration Efficiency of a Supernova Remnant

E. A. Helder,[1*] J. Vink,[1] C. G. Bassa,[2,3] A. Bamba,[4] J. A. M. Bleeker,[1,2] S. Funk,[5] P. Ghavamian,[6] K. J. van der Heyden,[7] F. Verbunt,[1] R. Yamazaki[8]

Cosmic rays are the most energetic particles arriving at Earth. Although most of them are thought to be accelerated by supernova remnants, the details of the acceleration process and its efficiency are not well determined. Here we show that the pressure induced by cosmic rays exceeds the thermal pressure behind the northeast shock of the supernova remnant RCW 86, where the x-ray emission is dominated by synchrotron radiation from ultrarelativistic electrons. We determined the cosmic-ray content from the thermal Doppler broadening measured with optical spectroscopy, combined with a proper-motion study in x-rays. The measured postshock proton temperature, in combination with the shock velocity, does not agree with standard shock heating, implying that >50% of the postshock pressure is produced by cosmic rays.

The main candidates for accelerating cosmic rays up to at least 10^{15} eV are shell-type supernova remnants (SNRs), which are the hot, expanding plasma shells caused by exploded stars (supernovas). To maintain the cosmic-ray energy density in the Galaxy, about three supernovae per century should transform 10% of their kinetic energy in cosmic-ray energy. Indeed, ~10^{14} eV electrons have been detected at forward shocks (*1*, *2*) and possibly at reverse shocks (*3*, *4*) of several shell-type remnants by their x-ray synchrotron emission, and particles with TeV energies have been detected in several SNRs by Cherenkov telescopes (*5*, *6*).

If SNRs transform a substantial amount of their kinetic energy into cosmic rays, this should affect the kinematics of the remnant. One imprint of energy losses by cosmic rays is a higher compression factor of the postshock plasma (*7*), for which indications have been found in both the Tycho SNR and SN 1006 (*8*, *9*). Another signature of the energy absorbed by cosmic rays is a lower postshock temperature (*10*–*13*). For shocks with conservation of mass, momentum, and energy, in the absence of cosmic rays, the postshock temperature (T_i) for species with mass m_i relates to the shock velocity (v_s) as

$$kT_i = \frac{3}{16} m_i v_s^2 \qquad (1)$$

in the case of no thermal equilibrium (i.e., the several atomic species do not have the same temperature), in which protons carry most of the thermal energy. In the case of fast thermal equilibration, this relation becomes $kT = \frac{3}{16}\mu m_p v_s^2$ ($\mu \cong 0.6$ for cosmic abundances). Indications for a lower postshock electron temperature have been found in the Magellanic Cloud remnant 1E 0102-72 (*14*), which may constitute only a minor part of the thermal pressure. Here we derive the postshock proton temperature and the shock velocity of the northeast rim of the shell-type SNR RCW 86 based on optical and x-ray observations.

RCW 86 (*15*) was detected in TeV energies by the HESS telescope (*16*) and is probably the remnant of the supernova witnessed by Chinese astronomers in 185 C.E. (*17*, *18*). It has been suggested that it evolves in a stellar-wind–blown cavity, where the southwest corner has already hit the cavity wall (*19*). The northeast side still expands in a less dense medium, and its x-ray spectrum is dominated by synchrotron radiation, which is an indication of efficient cosmic-ray acceleration.

The optical spectrum of the northeast rim of RCW 86 is dominated by hydrogen lines, with no [NII] line emission (*20*). The lack of [NII] indicates that the hydrogen line emission is not a result of strong cooling, but results from excitation processes immediately behind the shock front. The hydrogen lines from these shocks consist of two superimposed Gaussian line profiles: One, caused by direct excitation, has the thermal width of the interstellar medium (ISM), whereas the other is emitted after charge exchange between hot postshock protons and cold incoming neutral hydrogen and hence has the thermal width of the postshock protons. Hα emission and efficient cosmic-ray acceleration are likely to anticorrelate because incoming neutral species are likely to damp plasma waves, which are essential for shock acceleration (*21*) and because cosmic rays escaping ahead of the shock ionize the surrounding ISM and decrease the amount of Hα emission. In RCW 86, the Hα emission occurs all along the rim, including, although with weak emission, the parts coinciding with x-ray synchrotron emission, where efficient cosmic-ray acceleration is likely to occur

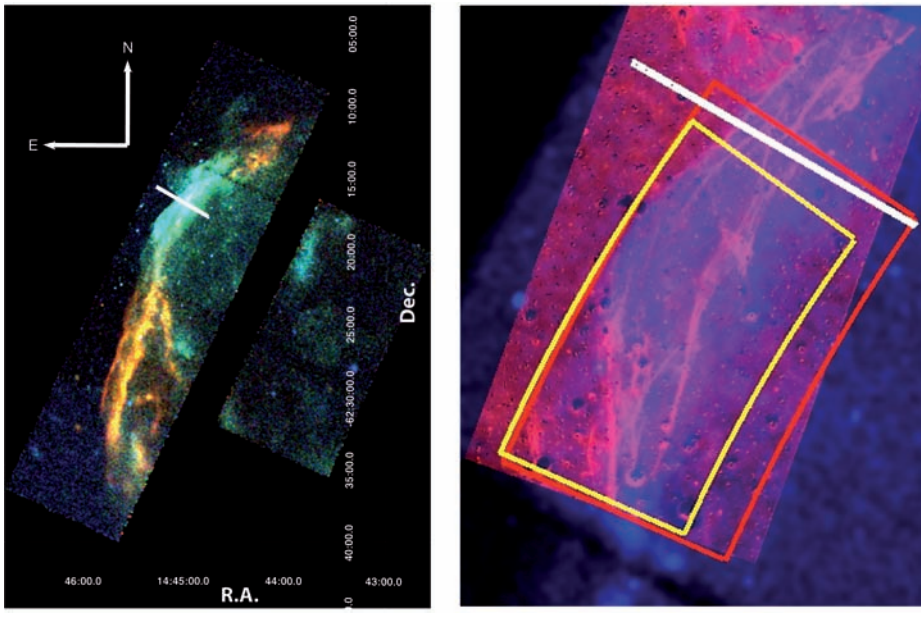

Fig. 1. (**Left**) The eastern rim of RCW 86, as observed in 2007 with Chandra. Red indicates the 0.5- to 1.0-keV band; green, the 1.0- to 1.95-keV band; and blue, the 1.95- to 6.0-keV band. The northern part has relatively more flux in the higher-energy bands, which is characteristic for synchrotron emission. (**Right**) Blue is the broadband keV Chandra image; red is the image as observed with the VLT through a narrow Hα filter. The regions (yellow and red) indicate where we measured the proper motion. In both panels, the location where we took the optical spectrum is indicated with a white line.

[1]Astronomical Institute Utrecht, Utrecht University, Post Office Box 80000, NL-3508 TA Utrecht, Netherlands. [2]SRON Netherlands Institute for Space Research, Sorbonnelaan 2, NL-3584 CA Utrecht, Netherlands. [3]Department of Astrophysics, Radboud University Nijmegen, Post Office Box 9010, Nijmegen, Netherlands. [4]Institute of Space and Astronautical Science–Japan Aerospace Exploration Agency, Department of High Energy Astrophysics 3-1-1, Yoshinodai, Sagamihara, Kanagawa 229-8510, Japan. [5]Kavli Institute for Particle Astrophysics and Cosmology, Stanford, CA 94025, USA. [6]Space Telescope Science Institute, 3700 San Martin Drive, Baltimore, MD 21218, USA. [7]Astronomy Department, University of Cape Town, Private Bag X3, Rondebosch 7701, South Africa. [8]Department of Physical Science, Hiroshima University, Higashi-Hiroshima, Hiroshima 739-8526, Japan.

*To whom correspondence should be addressed. E-mail: e.a.helder@uu.nl

(Fig. 1). The only other remnant in which Hα emission is seen all along the shell, including regions with x-ray synchrotron emission, is the SN 1006 SNR (*22*).

The right panel in Fig. 1 shows both the Hα and the x-ray emission of the northeast rim of RCW 86. The Hα emission marks the onset of the x-ray synchrotron radiation, which indicates that they are from the same physical system.

To measure the proton temperature, we used long-slit spectra obtained with the visual and near ultraviolet Focal Reducer and low-dispersion Spectrograph (FORS2) instrument on the Very Large Telescope (VLT) (*23*). We first imaged the northeast side of RCW 86, where the x-ray spectrum is dominated by synchrotron emission. Using this image as a guide, we pointed the slit at a location where the Hα emission is bright (Fig. 1 and table S1).

The spectrum's (Fig. 2) measured full width at half maximum is 1100 ± 63 km/s [see supporting online material (SOM) for further details], corresponding to a σ_v = 467 ± 27 km/s and implying a postshock temperature of 2.3 ± 0.3 keV.

To measure the shock velocity of the northeast rim of RCW 86, we observed it with the Chandra X-Ray Observatory in June 2007 and matched it with an observation taken in June 2004 (*18*). To make both observations as similar as possible, we used the same observation parameters as in 2004 (table S2). We measured the proper motion of the shock at the location of the slit of the Hα spectrum by comparing the positions of the shock in the two images (see SOM for further details). A solid estimate of the proper motion is 1.5 ± 0.5″ in 3 years' time (Fig. 3 and fig. S1), implying a shock velocity of (6.0 ± 2.0) × 10^3 km/s at a distance of 2.5 kpc (*24*, *25*). The statistical error on the measured expansion is on the order of 0.2″. However, when calculating the proper motions, we found that small details, such as slightly changing the angle in which we made the profile, tended to give a different proper motion, with a difference larger than the 0.2″ statistical error that we measured. However, in none of the measurements did we find a proper motion below 1.0″. Because the proper motion is higher than expected (*18*), we verified that it is consistent with data taken in 1993 with the Position Sensitive Proportional Counter (PSPC) on board the Roentgen Satellite (ROSAT) compared with the 2007 observation (Fig. 3 and fig. S1). Although the proper motion, using the nominal pointing of the ROSAT PSPC, is statistically highly significant, the large pointing error of ROSAT (~4″) results in a detection of the proper motion at the 2σ level.

Compared to other remnants of a similar age, the shock velocity is surprisingly high. Recent models (*26*) predict v_s ~ 5000 km/s after 2000 years for SNRs evolving in a wind-blown bubble (*27*). This fits with the scenario in which RCW 86 is evolving in a cavity and the southwest corner, which has a slower shock velocity (*28*, *29*) and a mostly thermal (*3*) x-ray spectrum, has already hit the cavity shell. Shock acceleration theory suggests that only shocks with velocities exceeding 2000 km/s emit x-ray synchrotron emission (*18*, *30*), which is also consistent with observations (*31*).

An additional uncertainty in the shock velocity is in the distance to RCW 86, which is based on converging but indirect lines of evidence. RCW 86 was found to be in the same direction as an OB association, at a distance of 2.5 kpc (*32*). Because high-mass stars are often found in such associations, the progenitor of RCW 86 may well have formed in this one, provided that RCW 86 is the remnant of an exploded massive star. Other studies (*24*, *25*) found a distance of 2.3 and 2.8 kpc, respectively, based on the line-of-sight velocity of ISM swept up by the remnant, combined with an observationally determined rotation curve of the Galaxy (*33*). The third argument supporting a distance of 2.5 kpc is the molecular supershell seen in CO emission in the direction of RCW 86, whose line-of-sight velocity agrees with that of RCW 86 (*34*). In further calculations, we take the distance toward RCW 86 to be 2.5 ± 0.5 kpc, leading to a shock velocity of 6000 ± 2800 km/s.

The relation between shock velocity and measured postshock proton temperature has been extensively studied (*20*, *29*, *35*–*37*), including the cross sections for excitation and charge exchange as function of v_s. Although recent studies show that there can be a substantial effect of cosmic rays on the postshock proton spectrum (*38*), until now, there was no need to include cosmic-ray acceleration in the interpretation of the postshock temperature, possibly because most of the Hα spectra are taken from the brightest rims of SNRs. Because Hα emission and efficient cosmic-ray acceleration are likely to anticorrelate (*21*), these rims probably have low cosmic-ray acceleration efficiency. A possible exception is "knot g" in the Tycho SNR, where indications for cosmic-ray acceleration in the form of a precursor have been found (*39*–*41*). Additionally, for some SNRs (*22*, *42*), the distance has been determined by using the postshock proton temperature in combination with the proper motion, using theoretical models that do not take into account energy losses and cosmic-ray pressure. This procedure leads to an underestimate of the distance if cosmic-ray acceleration is present. Thus, unless the distance is accurately determined in an independent way, there will be no discrepancy between the predicted v_s, based on *kT* and Eq. 1, and the actual shock velocity.

The shock velocity of the x-ray synchrotron rim implies a postshock temperature of 70 keV (assuming no thermal equilibrium) or 42 keV (assuming equilibrium), whereas the measured postshock temperature is 2.3 keV. This measurement is at least a factor 18 less than the postshock temperature estimated from the shock velocity, which can now be used to constrain current theoretical shock-heating models (*12*, *13*). Additionally, this proton temperature is close to the electron temperature at the same location (*18*), implying fast thermal equilibration between both species, breaking the trend between the shock velocity and the measure of thermal equilibrium seen in previous observations (*36*, *37*).

To translate this discrepancy into the energy and pressure in cosmic rays, we followed the approach of (*11*), which is based on standard shock equations for plane-parallel, steady-state shocks, modified by additional pressure and loss terms [see

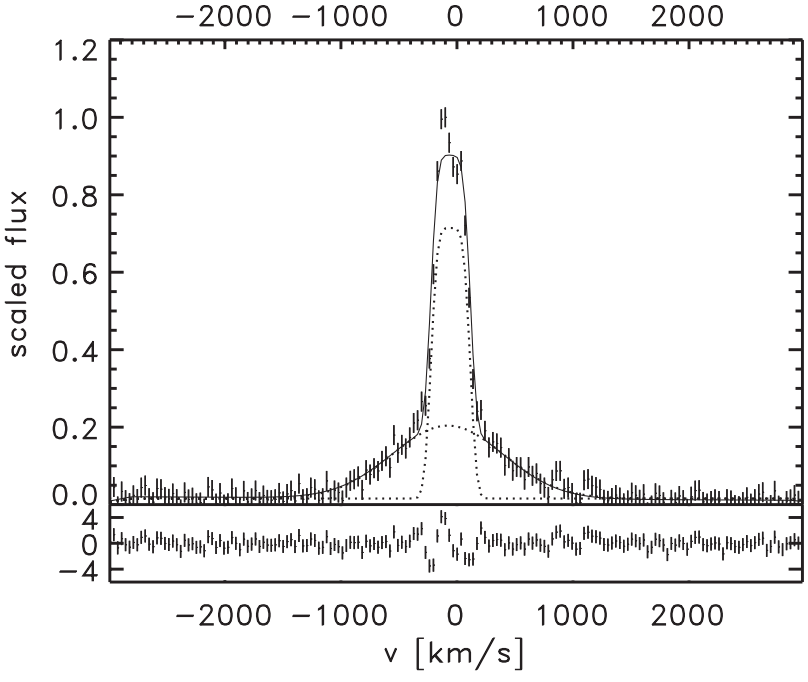

Fig. 2. The Hα spectrum, with broad and narrow components (dotted lines). The best-fitting spectrum is overplotted. The lower panel shows the residuals divided by the errors.

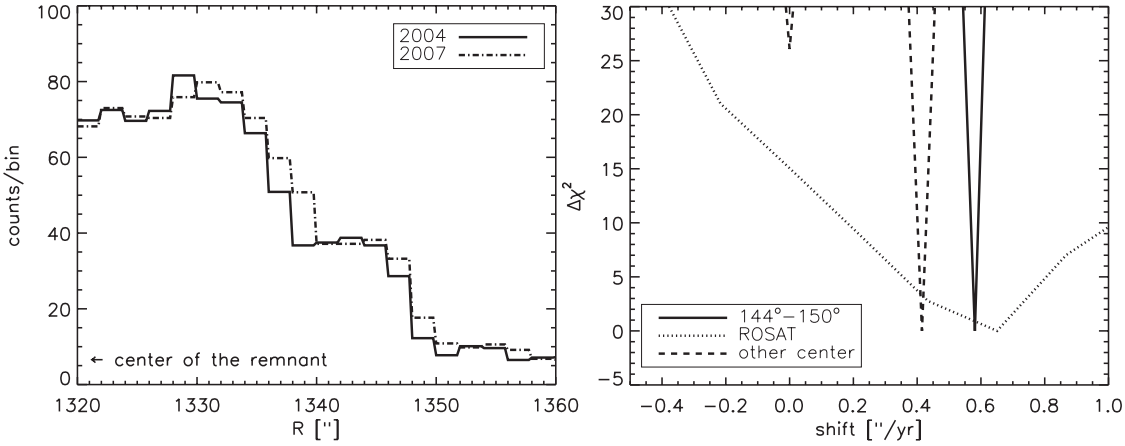

Fig. 3. (**Left**) Steep gradient in the radial profiles for the 2004 and 2007 observations, adaptively binned with the Haar method (*47*), so that each bin has a signal-to-noise ratio of at least 4, with a maximum bin width of 2″. (**Right**) χ^2 statistics of the proper motion measurement. (Details of the used radial profiles are in the SOM.)

also (*7*, *43*, *44*)]. The loss term is defined in terms of the incoming energy flux: $\varepsilon_{CR} \equiv F_{CR}/\frac{1}{2}\rho_0 v_s^3$, where F_{CR} is the amount of energy flux in cosmic rays that escapes from the system and ρ_0 is the preshock density. The parameter that indicates the fraction of the pressure induced by cosmic rays in the total postshock pressure is w_{CR} [$w_{CR} \equiv P_{NT}/(P_T + P_{NT})$], where P_T is the pressure in particles with a thermal and P_{NT} with a nonthermal energy distribution (i.e., CRs). We plot the modified equations (listed in the SOM) in Fig. 4 and indicate the region where the combination of kT and v_s of the northern rim of RCW 86 resides for thermal equilibrium as well as for no thermal equilibrium. As Fig. 4 shows, a postshock temperature and a shock velocity do not give a unique solution for w_{CR} and ε_{CR}. However, the cosmic rays significantly change the shock dynamics, because the combination solution is far away from $w_{CR} = 0$ and $\varepsilon_{CR} = 0$ (Fig. 4).

There are two ways to further constrain w_{CR} and ε_{CR}. First, an additional estimate of the compression ratio (χ) of the postshock plasma would exactly determine w_{CR} and ε_{CR}. For certain SNRs this is done by determining the distance between the supernova ejecta and the outer shock; a higher compression ratio implies that the swept-up ISM forms a thinner shell and hence the ejecta will be closer to the shock front (*8*, *9*). However, ejecta and swept-up ISM are distinguished only by their thermal spectra, which is (almost) absent in the x-ray synchrotron–dominated rim [~15% of the total x-ray emission (*18*)].

Another way is to invoke a dependency of w_{CR} on ε_{CR}. According to nonlinear shock acceleration theory (*12*, *45*), $\varepsilon_{CR}/w_{CR} = \frac{2}{\lambda}(1-1/\chi)^2$, in which χ is the compression ratio of the postshock plasma and $\lambda = 1,2$ indicates the (w_{CR},ε_{CR}) relation for a cosmic-ray spectrum with $f(p) \propto p^{-3}$,$p^{-3.5}$, respectively, with p the momentum of the cosmic rays. The $\lambda = 2$ line gives an upper limit to the energy losses, because it is valid for the most efficient cosmic-ray acceleration by cosmic-ray–modified shocks (*46*). For $f(p) \propto p^{-4}$, $\lambda = \ln(p_{max}/mc)$ (*12*), which can be large and does not provide a lower limit to ε_{CR}. Taking the $\lambda = 2$ line as an upper limit for ε_{CR}, we find a value for w_{CR} of $\geq$ 50%. One remaining question is whether we should include the effects of the turbulent magnetic field. The average magnetic field pressure in RCW 86 has been estimated to be $P_B = B^2/8\pi = 2.3 \times 10^{-11}$ dyn/cm^2, for a magnetic field of 24 μG (*18*). This is an order of magnitude below the thermal pressure, which we estimate to be $P_T = nkT = 3.7 \times 10^{-10}$ dyn/cm^2, for $n = 0.1$ (*18*) and $kT = 2.3$ keV. In reality, the magnetic field pressure may be higher if one takes full account of its unknown, turbulent spectrum.

In summary, our observations show that the postshock temperature of the northeast rim of RCW 86 is lower than expected from standard shock relations using the measured shock velocity. The high velocity (6000 ± 2800 km/s) of the shock implies a local low ISM density, which can be expected in a cavity blown by a stellar wind. Cosmic-ray acceleration decreases the postshock proton temperature in RCW 86 by a factor of 18, implying that ≥50% of the postshock pressure is due to cosmic rays.

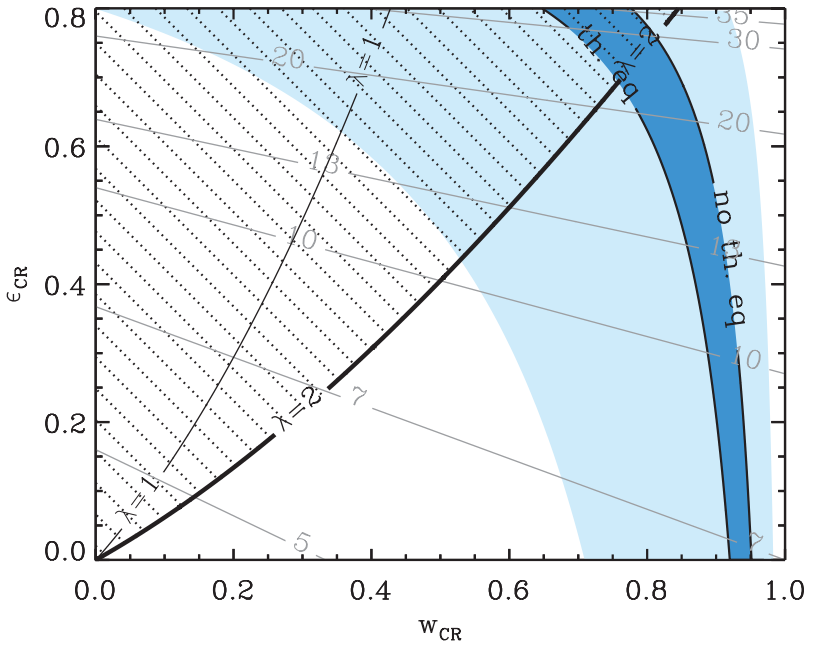

Fig. 4. Measurements of the shock velocity and postshock proton temperature for the northeast shock of RCW 86 in terms of w_{CR} and ε_{CR}. The dark blue area is the area allowed according to the modified equations, limited by full thermal equilibrium and no thermal equilibrium for the nominal values of kT = 2.3 keV, v_s = 6000 km/s. The light blue area shows the area of the kT and v_s with all uncertainties taken into account. The thin lines indicate the compression ratio (χ) of the postshock plasma. Within the allowed region, $\lambda = 2$ line provides an upper limit on ε_{CR} and a lower limit on w_{CR}.

References and Notes

1. K. Koyama *et al.*, *Nature* **378**, 255 (1995).
2. A. Bamba, R. Yamazaki, T. Yoshida, T. Terasawa, K. Koyama, *Astrophys. J.* **621**, 793 (2005).
3. J. Rho, K. K. Dyer, K. J. Borkowski, S. P. Reynolds, *Astrophys. J.* **581**, 1116 (2002).
4. E. A. Helder, J. Vink, *Astrophys. J.* **686**, 1094 (2008).
5. F. A. Aharonian *et al.*, *Nature* **432**, 75 (2004).
6. J. Albert *et al.*, *Astron. Astrophys.* **474**, 937 (2007).
7. E. G. Berezhko, D. C. Ellison, *Astrophys. J.* **526**, 385 (1999).
8. J. S. Warren *et al.*, *Astrophys. J.* **634**, 376 (2005).
9. G. Cassam-Chenaï, J. P. Hughes, E. M. Reynoso, C. Badenes, D. Moffett, *Astrophys. J.* **680**, 1180 (2008).

10. A. Decourchelle, D. C. Ellison, J. Ballet, *Astrophys. J.* **543**, L57 (2000).
11. J. Vink, in *High Energy Gamma-Ray Astronomy: Proceedings of the 4th International Meeting on High Energy Gamma-Ray Astronomy* (American Institute of Physics, College Park, MD, 2008), vol. 1085, pp. 169–180.
12. L. O'C. Drury, F. A. Aharonian, D. Malyshev, S. Gabici, *Astron. Astrophys.* **496**, 1 (2009).
13. D. J. Patnaude, D. C. Ellison, P. Slane, *Astrophys. J.* **696**, 1956 (2009).
14. J. P. Hughes, C. E. Rakowski, A. Decourchelle, *Astrophys. J.* **543**, L61 (2000).
15. G315.4-2.3, MSH 14-*63*.
16. F. Aharonian *et al.*, *Astrophys. J.* **692**, 1500 (2009).
17. F. R. Stephenson, D. A. Green, *Historical Supernovae and Their Remnants*, International Series in Astronomy and Astrophysics, vol. 5 (Oxford Univ. Press, Oxford, 2002).
18. J. Vink *et al.*, *Astrophys. J.* **648**, L33 (2006).
19. J. Vink, J. S. Kaastra, J. A. M. Bleeker, *Astron. Astrophys.* **328**, 628 (1997).
20. R. A. Chevalier, R. P. Kirshner, J. C. Raymond, *Astrophys. J.* **235**, 186 (1980).
21. L. O'C Drury, P. Duffy, J. G. Kirk. *Astron. Astrophys.* **309**, 1002 (1996).
22. P. F. Winkler, G. Gupta, K. S. Long, *Astrophys. J.* **585**, 324 (2003).
23. I. Appenzeller *et al.*, *Messenger* **94**, 1 (1998).
24. M. Rosado, P. Ambrocio-Cruz, E. Le Coarer, M. Marcelin, *Astron. Astrophys.* **315**, 243 (1996).
25. J. Sollerman, P. Ghavamian, P. Lundqvist, R. C. Smith, *Astron. Astrophys.* **407**, 249 (2003).
26. V. V. Dwarkadas, *Astrophys. J.* **630**, 892 (2005).
27. The effects of cosmic ray acceleration on the evolution of the forward shock are small; see (*13*).
28. K. S. Long, W. P. Blair, *Astrophys. J.* **358**, L13 (1990).
29. P. Ghavamian, J. Raymond, R. C. Smith, P. Hartigan, *Astrophys. J.* **547**, 995 (2001).
30. F. A. Aharonian, A. M. Atoyan, *Astron. Astrophys.* **351**, 330 (1999).
31. S. Katsuda, H. Tsunemi, K. Mori, *Astrophys. J.* **678**, L35 (2008).
32. B. E. Westerlund, *Astrophys. J.* **74**, 879 (1969).
33. J. Brand, L. Blitz, *Astron. Astrophys.* **275**, 67 (1993).
34. K. Matsunaga *et al.*, *Publ. Astron. Soc. Jpn.* **53**, 1003 (2001).
35. K. Heng, R. McCray, *Astrophys. J.* **654**, 923 (2007).
36. M. van Adelsberg, K. Heng, R. McCray, J. C. Raymond, *Astrophys. J.* **689**, 1089 (2008).
37. P. Ghavamian, J. M. Laming, C. E. Rakowski, *Astrophys. J.* **654**, L69 (2007).
38. J. C. Raymond, P. A. Isenberg, J. M. Laming, *Astrophys. J.* **682**, 408 (2008).
39. P. Ghavamian, J. Raymond, P. Hartigan, W. P. Blair, *Astrophys. J.* **535**, 266 (2000).
40. J.-J. Lee *et al.*, *Astrophys. J.* **659**, L133 (2007).
41. A. Y. Wagner, J.-J. Lee, J. C. Raymond, T. W. Hartquist, S. A. E. G. Falle, *Astrophys. J.* **690**, 1412 (2009).
42. R. C. Smith, R. P. Kirshner, W. P. Blair, P. F. Winkler, *Astrophys. J.* **375**, 652 (1991).
43. R. A. Chevalier, *Astrophys. J.* **272**, 765 (1983).
44. A. M. Bykov, K. Dolag, F. Durret, *Space Sci. Rev.* **134**, 119 (2008).
45. M. A. Malkov, L. Drury, *Rep. Prog. Phys.* **64**, 429 (2001).
46. M. A. Malkov, *Astrophys. J.* **511**, L53 (1999).
47. J.-L. Starck, F. Murtagh, A. Bijaoui, *Image Processing and Data Analysis. The Multiscale Approach* (Cambridge Univ. Press, Cambridge, 1998).

48. We thank A. Achterberg for a useful discussion of the current literature on the theory of shock heating. E.A.H. and J.V. are supported by the Vidi grant to J.V. from the Netherlands Organization for Scientific Research (NWO). This work was supported in part by Grant-in-Aid for Scientific Research from the Japanese Ministry of Education, Culture, Sports, Science and Technology, no. 194014 (A.B.) and no. 19047004 and 21740184 (R.Y.). S.F. is supported by Smithsonian Astrophysical Observatory grant G07-8073X. P.G. is supported by the Space Telescope Science Institute grant GO-11184.07. This paper is based in part on observations made with European Southern Observatory Telescopes at the Paranal Observatories under program ID 079.D-0735.

Supporting Online Material

www.sciencemag.org/cgi/content/full/1173383/DC1
SOM Text
Fig. S1
Tables S1 and S2
References

11 March 2009; accepted 15 June 2009
Published online 25 June 2009;
10.1126/science.1173383
Include this information when citing this paper.

Emulation of a Quantum Spin with a Superconducting Phase Qudit

Matthew Neeley,[1] Markus Ansmann,[1] Radoslaw C. Bialczak,[1] Max Hofheinz,[1] Erik Lucero,[1] Aaron D. O'Connell,[1] Daniel Sank,[1] Haohua Wang,[1] James Wenner,[1] Andrew N. Cleland,[1] Michael R. Geller,[2] John M. Martinis[1]*

In quantum information processing, qudits (*d*-level systems) are an extension of qubits that could speed up certain computing tasks. We demonstrate the operation of a superconducting phase qudit with a number of levels *d* up to *d* = 5 and show how to manipulate and measure the qudit state, including simultaneous control of multiple transitions. We used the qudit to emulate the dynamics of single spins with principal quantum number *s* = 1/2, 1, and 3/2, allowing a measurement of Berry's phase and the even parity of integer spins (and odd parity of half-integer spins) under 2π-rotation. This extension of the two-level qubit to a multilevel qudit holds promise for more-complex quantum computational architectures and for richer simulations of quantum mechanical systems.

Quantum computers are typically thought of as being composed of qubits, or two-level quantum systems (*1*). However, one can also use qutrits (three-level systems) or more generally qudits (*d*-level systems), which can simplify some quantum computations (*2*, *3*) and improve quantum cryptography (*4*). The advantages of qudits are also evident when one considers using a quantum computer not to perform computations but rather to emulate another quantum system by the direct implementation of an analogous physical Hamiltonian. This requires a map between the Hilbert space and unitary operators of the emulator and the target system. If the target system contains parts with $d > 2$ levels, then it maps much more naturally to a set of qudits, making a qudit emulator potentially more efficient.

We describe the operation of a superconducting phase qudit with full unitary control and measurement of the state (*5*, *6*). This device, one of a family of superconducting quantum information–processing devices (*7*), is typically operated as a qubit (*8*, *9*) by restricting it to the two lowest-energy eigenstates. By relaxing this restriction, we can operate it as a qudit in which the number of levels *d* can be chosen as desired, in this case up to $d = 5$.

Emulation of spin, or intrinsic angular momentum, naturally calls for qudits with $d > 2$. A spin state is described by two quantum numbers (*10*), the principal quantum number $s = 0, 1/2, 1, 3/2,...$ and the azimuthal quantum number *m*, limited to the $d = 2s + 1$ values $m = s, s - 1,..., -s$. For a given *s*, the general spin states $|\psi\rangle = \sum_m c_m|s,m\rangle$ span a *d*-dimensional Hilbert space, so that although qubits can be used to model spin-1/2 physics a qudit allows one to model spins $s \geq 1$ ($d \geq 3$).

When rotated about a closed path (Fig. 1), a spin state $|s,m\rangle$ acquires a phase factor $\exp(-im\Omega)$, where Ω is the solid angle enclosed by the path, as predicted by Berry (*11*–*13*). For a 2π-rotation ($\Omega = 2\pi$), integer spins are unchanged, whereas half-integer spins are multiplied by −1. This parity difference leads to the symmetric statistics of bosons (or antisymmetric statistics of fermions) under exchange, as described by the spin-statistics theorem (*14*, *15*). The effect of 2π-rotations was first observed on spins $s = 1/2$ via neutron interferometry (*16*, *17*) and later for $s = 1$ and $s = 3/2$ in nuclear magnetic resonance (*18*). In superconducting qubits, the spin-1/2 parity (*19*) and Berry's phase (*20*) have been measured. We measured Berry's phase and spin parity for spin-1/2, spin-1, and spin-3/2 at all solid angles using our qudit emulation (*21*).

Our flux-biased phase qudit (Fig. 2A) is a nonlinear resonator formed by a Josephson junction, inductor, and capacitor. Applied magnetic flux produces a cubic potential as a function of the junction phase δ, with barrier height ΔU that can be tuned so as to change the number of energy levels in the well (Fig. 2B). The cubic anharmonicity is crucial for qubit operation (*22*), allowing microwaves at frequency $\omega_{10} = (E_1 - E_0)/\hbar$ to drive transitions between $|0\rangle$ and $|1\rangle$ while minimizing "leakage" to $|2\rangle$ and higher (*23*). For measurement, a brief current pulse $I^{(1)}_{\mathrm{meas}}$ is ap-

[1]Department of Physics, University of California at Santa Barbara (UCSB), Santa Barbara, CA 93106, USA. [2]Department of Physics and Astronomy, University of Georgia, Athens, GA 30602, USA.

*To whom correspondence should be addressed. E-mail: martinis@physics.ucsb.edu